Acta Polytechnica **59**(4):423–434, 2019
DOI:10.14311/AP.2019.59.0423
© Czech Technical University in Prague, 2019
available online at https://ojs.cvut.cz/ojs/index.php/ap

COMMON CROSSING CONDITION MONITORING WITH ON-BOARD INERTIAL MEASUREMENTS

Mykola Sysyn[a,*], Olga Nabochenko[b], Ulf Gerber[a], Vitalii Kovalchuk[b], Oleksiy Petrenko[c]

[a] *Technical University of Dresden, Transport Faculty, Department of Planning and Design of Railway Infrastructure, Hettnerstrasse 1/3, D-01069, Dresden, Germany*

[b] *Dnipro National University of Railway Transport, Lviv Faculty, Department of Rolling Stock and Track, Blagkevich 12a, 79052, Lviv, Ukraine*

[c] *Lviv Polytechnic National University, Institute of Civil and Environmental Engineering, Department of Construction Industry, Bandery str. 12, 79013, Lviv, Ukraine*

[*] corresponding author: mykola.sysyn@tu-dresden.de

Abstract. A railway turnout is an element of the railway infrastructure that influences the reliability of a railway traffic operation the most. The growing necessity for the reliability and availability in the railway transportation promotes a wide use of condition monitoring systems. These systems are typically based on the measurement of the dynamic response during operation. The inertial dynamic response measurement with on-board systems is the simplest and reliable way of monitoring the railway infrastructure. However, the new possibilities of condition monitoring are faced with new challenges of the measured information utilization. The paper deals with the condition monitoring of the most critical part of turnouts - the common crossing. The application of an on-board inertial measurement system ESAH-F for a crossing condition monitoring is presented and explained. The inertial measurements are characterized with the low correlation of maximal vertical accelerations to the lifetime. The data mining approach is used to recover the latent relations in the measurement's information. An additional time domain and spectral feature sets are extracted from axle-box acceleration signals. The popular spectral kurtosis features are used additionally to the wavelet ones. The feature monotonicity ranking is carried out to select the most suited features for the condition indicator. The most significant features are fused in a one condition indicator with a principal component analysis. The proposed condition indicator delivers an almost two-time higher correlation to the lifetime as the maximal vertical accelerations. The regression analysis of the indicator to the lifetime with an exponential fit proves its good applicability for the crossing residual useful life prognosis.

Keywords: Common crossing, on-board inertial measurement, condition indicator, feature ranking, data fusion, principal component analysis.

1. Introduction

The competitiveness of the railway transportation comparing to other transportation systems is significantly influenced with the renewal and maintenance costs of the railway infrastructure. The major part of the infrastructure maintenance costs are the track maintenance costs [1]. The railway turnout is a comparatively low-cost part of the railway superstructure that shares about 10 % of the superstructure investment costs [1]. Nevertheless, at the same time, the renewal and maintenance costs of turnouts share up 50 % of the track maintenance costs because of the disproportionately short lifecycle of turnouts. An ordinary track has up to 5-10 times higher lifetime than railway turnouts. Another cost driver of the turnout maintenance is relatively expensive inspection works. According to [2] 50 %, of the overall maintenance costs for switches and crossings (S&C) on Deutsche Bahn (DB) are the costs for inspection, service and test measures. These are thus the main cost drivers due to comparative frequent inspections with a relatively low automatisation. The inspection of a common crossing is usually executed by a visual inspection and manual geometry measurements of the frog nose and wing rail. Therefore, the diagnostic systems with automated measurement and monitoring of S&C are a promising way towards the reduction of the cost driver, and therefore, the increase of competitiveness of the railway transportation overall. Different track-side and on-board systems for railway track condition monitoring are used nowadays. On-board systems have the advantage to monitor the long track distance and large number of track turnouts, etc., with a one measurement system. Moreover, on-board systems on operational trains provide the additional benefit that consists in the replacement of cost expensive measurement trains. The most of on-board measurement systems are based on inertial measurements of accelerations on axle-box or car bodies [3].

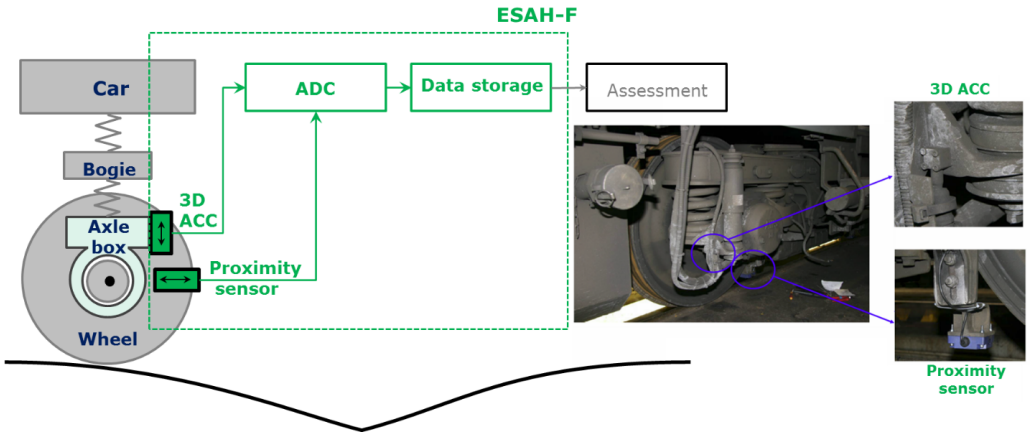

Figure 1. On-board inertial measurement system ESAH-F [4]

At present, there are a lot of studies related to the application of track condition monitoring systems [5–9]. The paper deals with the inertial measurements of the system ESAH-F (Electronic Analysis System of Crossing – Portable) that is tested on German railways (DB AG). The ESAH-F (Figure 1) on-board system is used for the common crossing monitoring of turnouts [4]. The main parts of the system are 3D acceleration sensors (ACC) that are located on axle-boxes of one bogie of passenger operational trains. A proximity sensor is used for an additional GPS accurate positioning of common crossings and controlling the ACC sensor measurement. The measured acceleration and proximity signals are preprocessed, digitalized and stored in a cloud.

A rail discontinuity on common crossing causes the increased accelerations that appear while trains pass on crossing. Figure 2 explains the formation of the geometrical irregularities due to the rail discontinuity. During the movement of the wheel along the wing rail, due to the wheel profile conicity, the wheel contact point moves outside from the wheel longitudinal trajectory (line 1-2). At the same time, the wheel moves down until the contact point 3 of the wheel profile with the frog rail appears. After that, the wheel rolls up again on the primary level due to the elevation of the frog rail longitudinal profile (line 3-4). The vertical position of the wheel during the passing consists of the crossing is influenced by the structural and wear irregularities. The structural irregularity is a deviation from the nominal shape and the wear irregularity (Figure 2, points 5-6) appears during the crossing operation. Both the structural and the wear irregularities cause a dynamical interaction and wheel loadings that lead to an accelerated deterioration of rails, sleepers, fastenings and ballast layer. The problem of the crossing condition monitoring, unlike the one of the ordinary track, is to estimate the measured inertial impact changes upon the already high initial values of acceleration.

Despite the obvious advantages of on-board monitoring systems on operational trains, there are a lot of significant drawbacks that limit the wide applications of the systems in the railway transportation. The main one is the low quality of the measured information. The measured axle-box accelerations depend not only on the track state but also on the wheel state, stiffness in track and train suspension, train velocity, axle of sensor position, etc. Additionally, the operational trains with on-board measurement systems are usually limited to light passenger trains that could not depict the real loading of freight trains in mixed traffic. The low information quality of the measurements makes it difficult to utilise them for the track condition monitoring. The conventional analysis method of a maximal acceleration consideration shows a relatively low relation to the lifetime. Figure 3 shows the change of maximal vertical accelerations during the crossing lifecycle. The random variation of the maximal vertical acceleration is compared with the systematic change of the measured parameter. The correlation coefficient is relatively low and is much lower in the region until the first rail contact fatigue (RCF) damages occur, since about a half of the systematic acceleration growth is caused by the damages itself.

The application of advanced information processing and analysis methods could solve the problem. The modern signal processing and statistical learning science provides a wide range of methods for deeper information exploration and recovering of hidden relations in the same information. Indeed, the maximal accelerations or similar analysis measures contain a tiny amount of information compared to the information volume of raw measured signals. Many recent studies in transportation are focused on the problem of the structural health and condition monitoring with machine and deep learning information processing. A widespread overview of the theoretical and practical techniques of a contemporary data science analysis with application to railway track engineering is presented in [10]. The application of sequential feature selection within the machine learning approach for on-board axle-box inertial measurements of operational

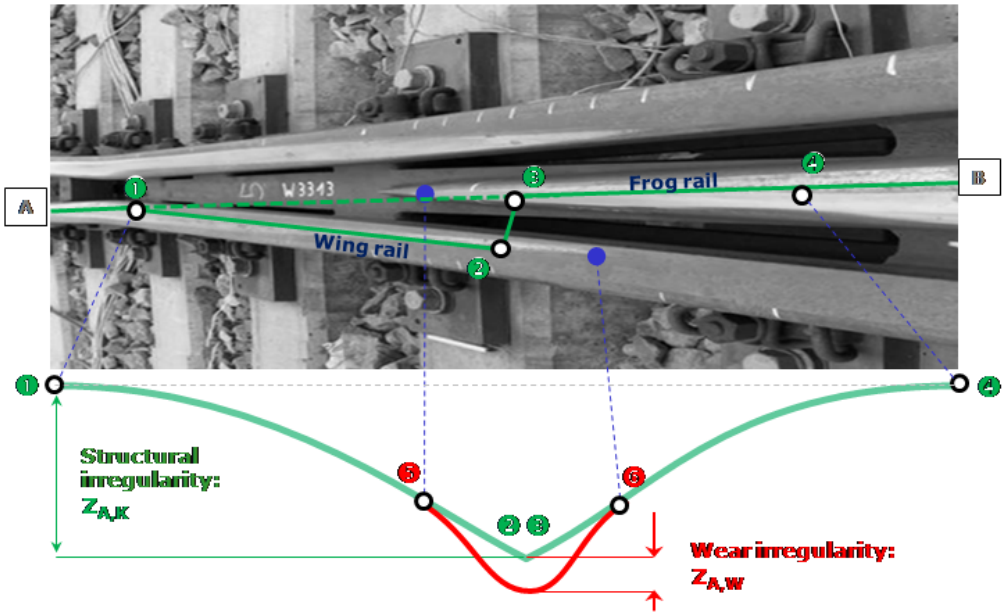

FIGURE 2. Geometrical irregularities in common crossing

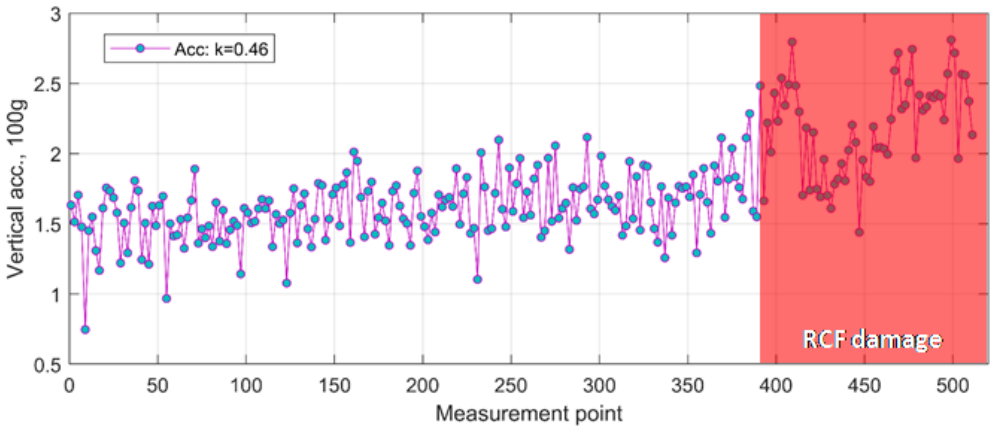

FIGURE 3. The progress of measured maximal vertical accelerations during crossing lifecycle

trains is proposed in [11]. The parameters for the turnout monitoring with the application track-side inertial measurements were considered in the study [12]. The monitoring of a railway superstructure in transition zones from ballast to ballast-less track with a prediction of quality development is presented in [13, 14]. The statistics based feature selection for an evaluation of railway ballast consolidation is proposed in [15]. The application of supervised and unsupervised machine learning techniques within the track geometry big data analysis is discussed in [16]. A combination of statistical and mechanical approach for a common crossing fault prediction with track-side inertial measurements is shown in [17]. The reinforcement learning for the improvement of the disturbance parameters determination in the railway operational simulation is proposed in [18]. A physical modelling of an on-board inertial measurement system for a detection of track geometry failures is presented in [19]. Prediction of RCF on the frog rail using machine learning methods and image processing of magnet particle inspections is demonstrated in [20]. The studies of track and switches component damages due to different failure modes are presented in [21, 22]. A cause analysis of the RCF damage on a frog rail of a common crossing is demonstrated in [23]. The analysis is based on track-side acceleration and profile measurements of the common crossing during its overall lifecycle. A crossing structural health analysis and lifecycle prediction using the track-side monitoring and machine learning methods is presented in [24]. The goal of the present paper consists in a development of a common crossing indicator that is based on the measured vertical acceleration of axle-box and could best describe the relation to the crossing lifetime. The multiple feature extraction from time and frequency domains, feature ranking and fusion with the principal component analysis (PCA) are used to reach the goal.

2. Data exploration and feature extraction

The axle-box acceleration measurements of the onboard system ESAH-F are analysed for the common crossing with a 1/12 crossing angle and rails UIC60 steel R350HT. The system was installed at 2 axleboxes of one bogie of operational passenger doubledecker trains. The spatial 3D accelerations were measured with a sampling rate of 50 kHz. The overall number of measurements is 528 together with 2 axlebox sensors on 2 axles. The crossing monitoring is carried out over the full lifecycle of the turnout of 282 days between two replacements. The measured data are not continuous in the crossing's lifetime – wide timespans with missing data are present. The measurement system ESAH-F has no exact longitudinal position measurement, therefore, the acceleration maximal points are used to synchronise different measurements. The measured signals are analysed in time and frequency domains with a continuous wavelet transform of the type "morlet". Figure 4 depicts the time series of the vertical acceleration and their wavelet diagram along the track coordinate for one measurement axle passing.

To utilise the measurement information more efficiently, the 3 groups of different features are extracted:

(1.) time domain features;

(2.) wavelet spectral features;

(3.) spectral kurtosis features

The maximal acceleration was conventionally used as a condition indicator of a common crossing in many studies [25]. However, the acceleration signal form is also changing during the lifetime of the crossing. The additional potential time domain features [26], [27] are extracted to quantify the signal form. The features are extracted from the signal window that includes the main part of vibrations due to the wheel and rail interaction in the crossing zone (Figure 4 above). Table 1 shows the description of the time domain feature set together with the abbreviations used.

Another group of features is derived from the frequency domain with a wavelet analysis. The features are determined as mean values of wavelet coefficients in the windows of different width and frequency (Figure 4, down). The separation of features corresponds to the local maxima zones at the wavelet diagram. The accepted window width takes into account the possible variation of the zones with high coefficient values due to the problem with a poor coordinate synchronisation. It could be mechanically interpreted as axle-box oscillations due to the impact loading, wheel irregularities, natural frequency of wheel-crossing mechanical system, rail wear irregularity wave, structural crossing irregularity and ballast settlement wave. The spectral features with their explanation are described in Table 2. Spectral kurtosis (SK) is one of the popular methods for the analysis of vibration signals from rotating machine parts. It is used to indicate and isolate the nonstationary or non-Gaussian process in the frequency domain. The advantage of the spectral kurtosis consists in finding the optimal frequency and bandwidth for recovering the demodulated impulsive signature that is hidden in the raw vibration waveform [28]. The spectral kurtosis SK(f) is calculated with a short-time Fourier transform (STFT) [29]:

$$SK(f) = \frac{\left\langle |S(t,f)|^4 \right\rangle}{\left\langle |S(t,f)|^2 \right\rangle^2} - 2 \qquad (1)$$

where *S(t,f)* - short-time Fourier transform of the acceleration time series signal $A(t)$ with a window function $w(t)$; $\langle - \rangle$ is the time-average operator.

Figure 5 shows the spectral kurtosis calculated for two windows width of the STFT in the same spectral range as the wavelet transform. The maximal values are used as spectral kurtosis features. The global maxima of the spectral kurtosis are located in the range of 10000-15000 Hz that could correspond to the wheel induced vibrations. The spectral kurtosis features are analogous to those of the time domain: mean value, standard deviation, skewness and kurtosis. The features are shown together with the wavelet spectral features in Table 2.

3. Feature ranking and selection

The extracted feature set is appended with the known operational conditions: train velocity and wheelset where the acceleration sensors are located. A preliminary analysis of the extracted feature correlation to the lifetime is carried out. Figure 6 shows the evolution of feature values and their correlation to the crossing lifecycle as well as the corresponding operational conditions variation. The feature values are normalized and centred to provide the comparable values of the relation to the lifetime. The figure 6 shows that the train velocities variate in the range of 100-160 km/h. The accelerations of bogie axles come together except of the final points of the statistics where accelerations of the second axle are not recorded. The highest linear correlations to the lifetime have the following time domain features: *Std*, *P2P*, *Energy*. The best spectral features are low frequency ones *spl1*, *spl2*, middle frequency feature *spm1* and high frequency feature *sph2*. However, many features have a nonlinear relation to the crossing lifetime that could make it more difficult to use them for the crossing condition estimation. The high frequency feature *sph2* has the highest growth during the final part of the lifecycle as well as many other features. Apparently, it could be explained with the influence of the additional dynamic interaction due to the RCF damage itself.

Additionally to the estimation of the feature suitability for the condition indication purpose with a

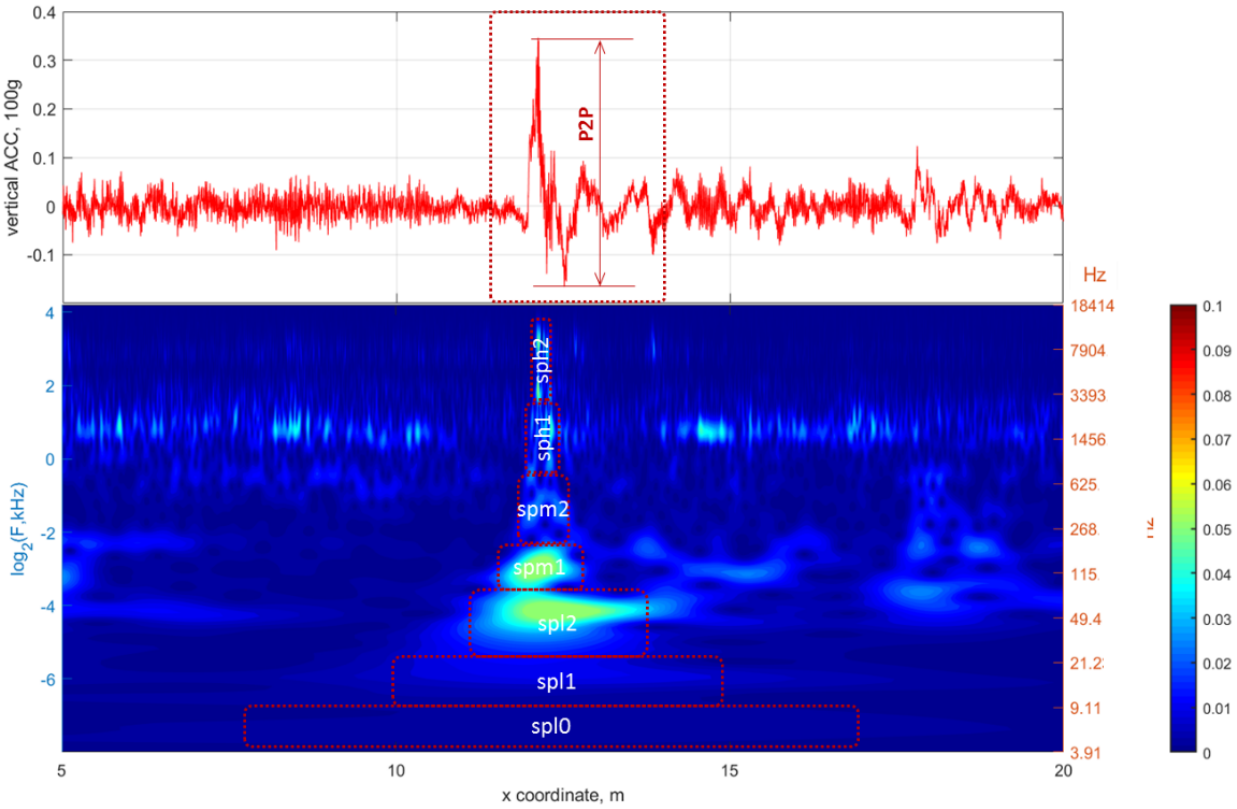

FIGURE 4. Time domain and spectral features from vertical acceleration (above) and wavelet coefficients (down)

Abbr.	Description	Formula
Mean	Mean vertical accelerations	$Mean = \frac{1}{N}\sum_{i=1}^{N} A_i$
Std	Standard deviation of vertical accelerations	$Std = \sqrt{\frac{1}{N-1}\sum_{i=1}^{N}(Ai - Mean)^2}$
Skew	Skewness - a measure of the asymetry of the data round the mean	$Skew = \frac{\frac{1}{N}\sum_{i=1}^{N}(Ai-Mean)^3}{\left(\sqrt{\frac{1}{N}\sum_{i=1}^{N}(Ai-Mean)^2}\right)^3}$
Kurt	Kurtosis - a measure of bulging or convexity	$Kurt = \frac{\frac{1}{N}\sum_{i=1}^{N}(Ai-Mean)^4}{\left(\sqrt{\frac{1}{N}\sum_{i=1}^{N}(Ai-Mean)^2}\right)^2}$
P2P	Peak-to-peak value - difference between the maximal positive and negative accelerations	$P2P = \max(Ai) - min(Ai)$
CrestF	Crest factor - ratio of peak values to the effective value of waveform	$CrestF = \frac{\max(Ai)}{\sqrt{\frac{1}{N}\sum_{i=1}^{N}(Ai-Mean)^2}})$
ShapeF	Shape form - ratio of variation to the effective mean value	$ShapeF = \frac{\sqrt{\frac{1}{N}\sum_{i=1}^{N}(Ai-Mean)^2}}{\frac{1}{N}\sum_{i=1}^{N}\lvert Ai\rvert})$
ImpF	Impulse factor - ratio of peak values to the effective mean value	$ImpF = \frac{\max(Ai)}{\frac{1}{N}\sum_{i=1}^{N}\lvert Ai\rvert})$
MargF	Margin factor - ratio of peak values to the square effective mean value	$MargF = \frac{\max(Ai)}{\left(\frac{1}{N}\sum_{i=1}^{N}\lvert Ai\rvert\right)^2})$
Energy	Signal energy	$Energy = \frac{1}{N}\sum_{i=1}^{N}(Ai)^2)$
MargF	Margin factor - ratio of peak values to the square effective mean value	$MargF = \frac{\max(Ai)}{\left(\frac{1}{N}\sum_{i=1}^{N}\lvert Ai\rvert\right)^2}$

TABLE 1. Time domain features.

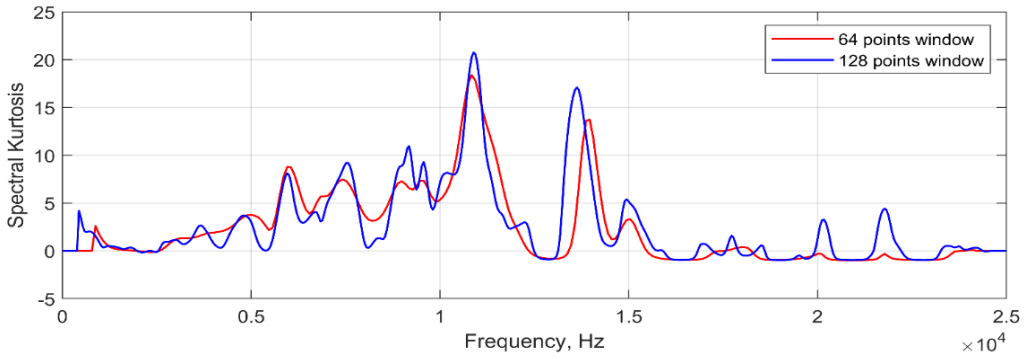

Figure 5. Spectral kurtosis for measured vertical acceleration

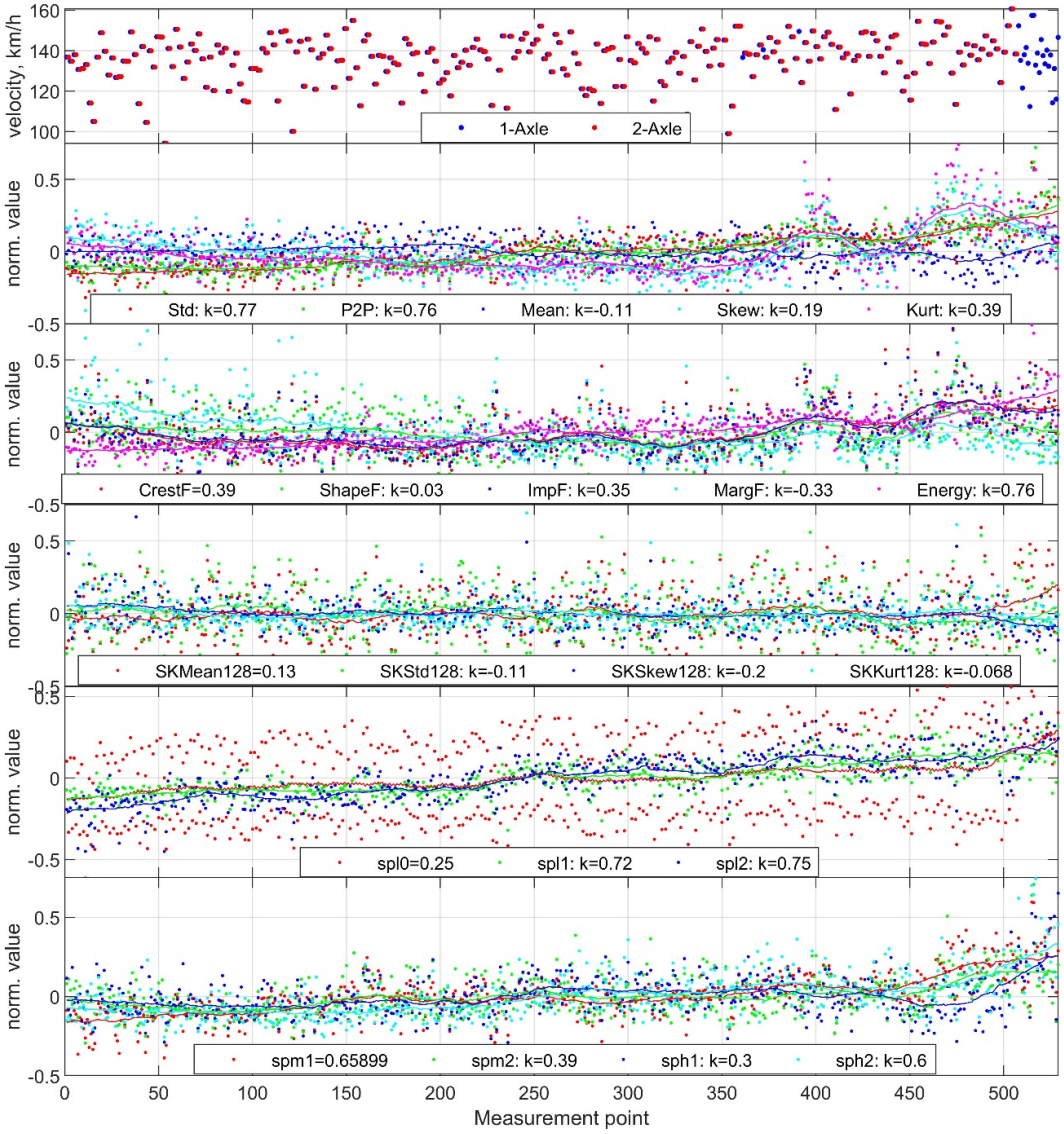

Figure 6. The progress of feature values and their correlation to crossing lifecycle

Abbr.	Description
spl0	Wavelet power spectral density for the low frequency range 3-10 Hz near impact point
spl1	Wavelet power spectral density for the low frequency range 10-30 Hz near impact point
spl2	Wavelet power spectral density for the low frequency range 30-80 Hz near impact point
spm1	Wavelet power spectral density for the middle frequency range 80-200 Hz near impact point
spm2	Wavelet powet spectral density for the middle frequency range 200-930 Hz near impact poinr
sph1	Wavelet power spectral densgty for the hiih frequency range 930-4000 Hz near impact point
sph2	Wavelet power spectral density for the high frequency range 4000-16000 Hz near impact point
SKMean64(128)	SK mean value fro the STFT window 64(128) points
SKStd64(128)	SK staniard deviation for the STFT window 64(128) points
SKSkew64(128)	SK skewhess for tne STFT window 64(128) points
SKKurt64(128)	SK kurtosis for the STFT window 64(128) points

TABLE 2. Wide table.

correlation criterion, the quantification of the importance of the features for the prognosis purpose is carried out. The monotonicity criterion is often used for the aim [30]. The monotonicity is calculated with the following formula:

$$MNCT = \frac{1}{M}\sum_{j=1}^{M}\left|\sum_{k=1}^{N_j-1}\frac{sgn\left(x_j\left(k+1\right)-x_j(k)\right)}{N_j-1}\right| \tag{2}$$

where x_j - measurement vector of the feature; N - number of measurement points; M - number of measurement sensors.

The feature ranking with the monotonicity criterion is depicted at Figure 7. The feature set *Std*, *Energy*, *spl2*, *spm1*, *P2P* and *spl1* can be selected in a separate group with significantly higher monotonicity parameters than other features. The group in sum encloses more monotonicity parameters than all other remaining features. Taking into account that the new features with a moderate monotonicity like *spm2*, *Skew* etc. are significantly nonlinear to the lifetime, the threshold 0.1 is taken for the feature selection. Thus, the 6 most significant features are selected for the following condition indicator development. The features *Std* and *Energy* are of the same physical background, they could be considered as permutable, and therefore, one feature Energy is taken into account for the following feature fusion.

4. Feature fusion with principal component analysis

A feature fusion is used to develop the condition indicator from the selected feature set. It is a process of combining the specific extracted features, which are transformed to one that is more informative. One of the most popular techniques for the data fusion or dimensionality reduction is the principal component analysis [31, 32]. It is an unsupervised learning technique that reduces the dimensionality of a feature set by transforming it to a smaller one with a low dimension representation. The PCA discovers linear dependencies between variables and replaces groups of correlated variables with new, uncorrelated variables that are known as principal components. The PCA can be formally notated as follows [33]:

$$X = W^T \cdot S \tag{3}$$

where X - the original feature set matrix with n-rows or observations and p- columns containing features; S - the principal component scores or matrix of transformed features; W - principal component loads.

The objective of the PCA is to find a linear combination of loadings and features with a maximum variance [34]:

$$w = \arg\max_{\|w\|_{2=1}} \sum_{i=1}^{n} \left(x_i^T w\right)^2 \tag{4}$$

The results of the PCA are shown in Figure 8, where the scores in a space of the first 3 most significant variation components PC1, PC2, PC3 are presented. Additionally, each point is highlighted with a colour

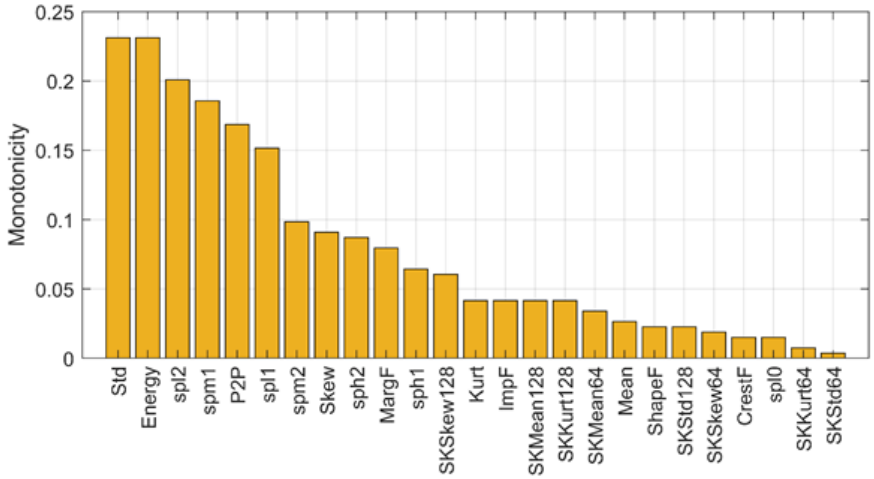

Figure 7. Feature monotonicity ranking

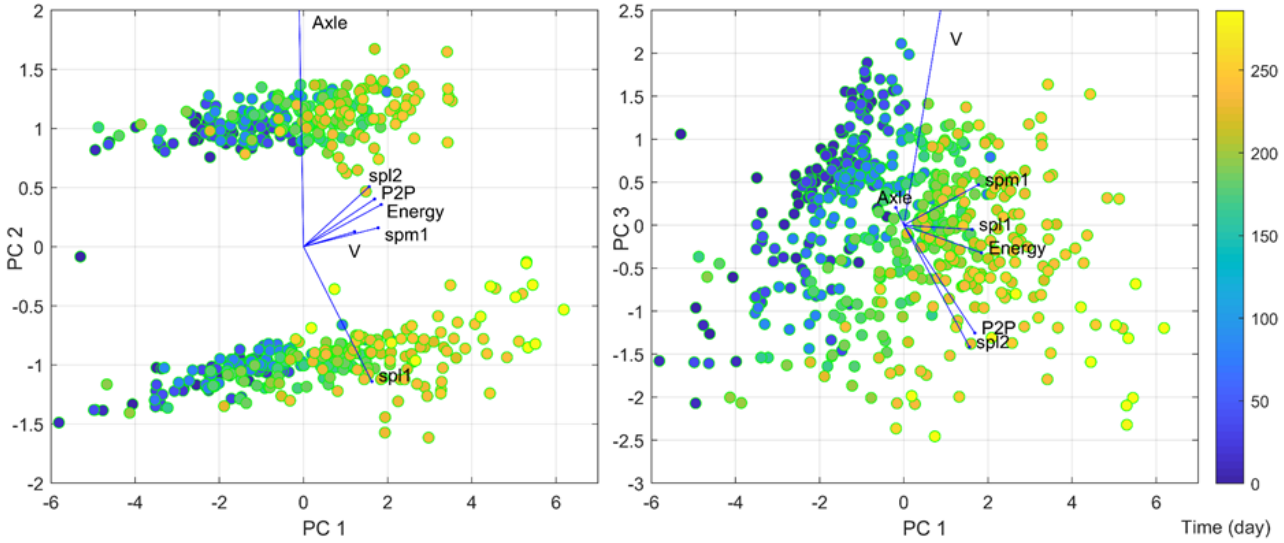

Figure 8. Crossing lifetime in PC1-PC2 space (left) and PC1-PC3 space (right)

that corresponds to the crossing lifetime. Furthermore, the biplot is appended to explain the direction of the influence of the initial feature set. The left diagram of the Figure 8 that shows the transformed variables in the first and second component space, demonstrates two groups of points. The groups correspond to the acceleration measurements of the first and second axles. The second component PC2 and the direction of the *Axle* feature on the biplot are almost collinear. The highest relation to the lifetime is in the direction of the first principal component PC1. The second principal component PC2 has a relatively negligible relation to the crossing lifetime. It could be explained by the fact that the PCA is a blind separation technique that does not take into account the response variable.

The right diagram of the Figure 8 shows the same relation from the viewpoint of the third principal component PC3. Here, the PC3 component has a lesser relation to the lifetime than the PC1, but also a significant one. The features *Energy* and *spl1* show the best direction of the lifetime variation. Figure 9 depicts the weight of each feature in the first and third components. All the features have the significant weight in the components except of the feature *Axle*. The feature is excluded from the following derivation of the common crossing condition indicator.

The fused condition indicators follow from the linear regression of principal components:

$$Y = S \cdot B + e \tag{5}$$

where Y - the response variable, or here, the lifetime of crossing, S - the predictor variables or here the PCA scores: $S = X = W^{-1}X$; B - the regression coefficients to be estimated; e - the errors or residuals.

Figure 10 demonstrates the progress of the condition indicator in normalized values during the crossing lifecycle. The correlation coefficient is almost two times higher than the one for the maximal vertical accelerations (Figure 3).

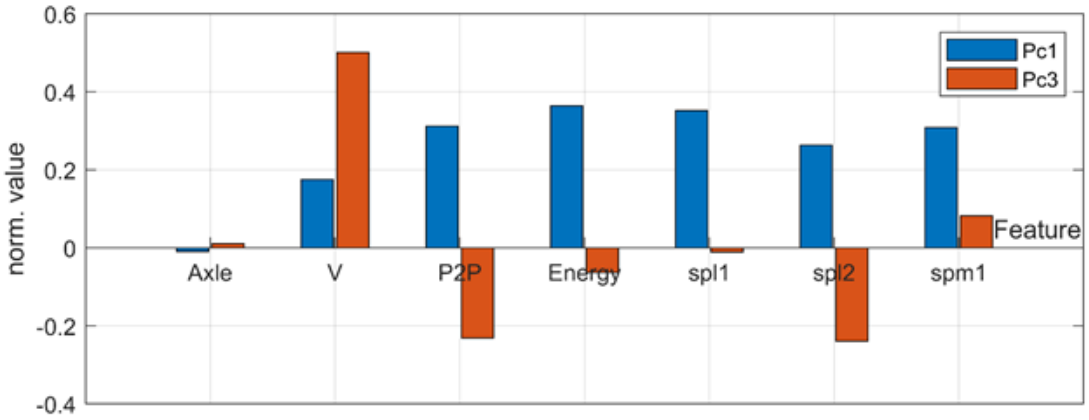

FIGURE 9. The weights of components PC1 and PC3 for selected features

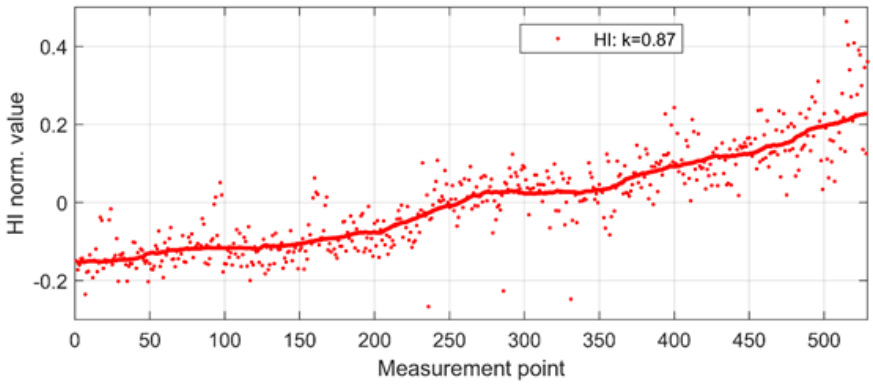

FIGURE 10. Crossing condition indicator variation over the measurements

The measured data are not continuously distributed over the crossing lifetime. Figure 11 shows the condition indicator of a common crossing relating to all lifetime days. The seemingly random variations of the indicator at Figure 10 can be fitted well with the exponential relation. The 95% function prediction bounds show a relatively low uncertainty of prediction that is less than 8% when compared to the explained indicator variation. However, the observation variation reaches up to 40% of the value, which does not diminish the developed condition indicator. The averaging of the indicator values to one day or week could provide a much stable estimation of the common crossing condition.

5. DISCUSSION

A condition monitoring of the S&C is more complicated than that of an ordinary railway track due to high loadings of wheels already at the beginning of the lifecycle and the relatively insignificant growth of the loading until the first RCF damages appear. For a more efficient utilisation of information from axlebox acceleration measurements, more features were extracted. The overall feature set contains 21 time-domain and spectral features. There are more features that could be additionally extracted from both the time and frequency domain, but it would not avoid the inherent problems of the extraction. The time domain features are extracted in a constant window to take into account only the crossing zone interaction. However, the interaction zones at the beginning and at the end of the lifetime have a different size. The criteria for the optimal window size could improve some feature results. The poor coordinate synchronisation with the maximal acceleration points makes it difficult to compare the time-spectral features from the wavelet transform. The wider windows with the coefficient averaging are used to avoid the problem. However, it leads to a reduction of the feature significance. The automated identification of a feature location would be useful as an intermediate step before the spectral feature extraction. The relatively poor relation of the spectral kurtosis feature set to the lifetime could be explained with the meaningful high local frequencies 10-15 kHz taken into account. That does not correspond to the other spectral features, where the main relation to the lifetime lies in the low and middle frequency range. The means of the SK features are low and have an almost linear relation to the lifetime (Figure 6). It could be supposed that the extracted SK features are rather related to the wheel surface condition, since the application field of the SK

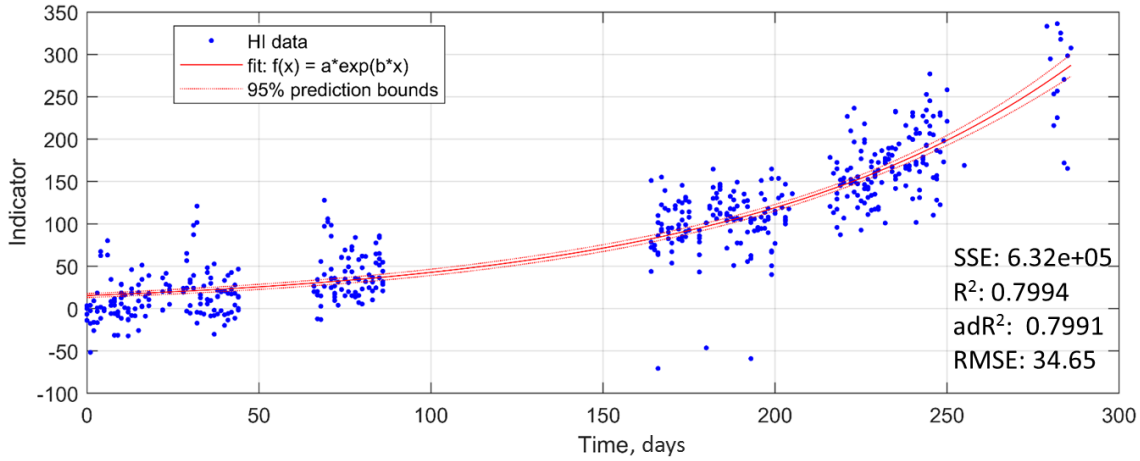

Figure 11. Crossing condition regression during its lifecycle time

is traditionally used for vibration signals of rotating machine parts, like bearing or wheels. Nevertheless, the negative results with the SK application could potentially be used in future studies for a wheel influence separation. Another way for improving the condition indicator is taking into account another 2 acceleration components in the longitudinal and lateral directions from all 4 ACC sensors. Taking into account the additional operational conditions like the train movement direction relatively to the turnout, crossing longitudinal profile, etc., could also contribute to the perfection of the crossing condition estimation. Despite the sufficient results received in the present study with the developed condition indicator for the crossing monitoring, there are two basic problems inherent to on-board condition monitoring from operational trains:

- The measured dynamic impact on operational passenger trains cannot depict the real loading of mixed traffic, where the freight trains are the dominating factor in the crossing deterioration.
- The change of the crossing condition indicator during its lifetime cannot be explicitly associated with the deterioration of separate crossing parts like the RCF, rail wear, fastenings, sleeper deterioration or ballast settlements.

The present study should be considered as a step towards the solution of the considered problems as well as the crossing remaining life prognosis.

6. Conclusions

The paper presents an approach of a common crossing condition indicator development based on machine learning methods. The following main results can be concluded:

(1.) The most significant time-domain features are *Std*, *Energy* and *P2P*.

(2.) The most significant spectral features are *spl1*, *spl2* and *spm1* that correspond to a frequency range of 10-200 Hz.

(3.) The spectral kurtosis features have an insignificant relation to the crossing lifetime.

(4.) The influence of the axle sensor location has an insignificant influence on the condition estimation results.

(5.) The proposed condition indicator provides an almost twotimes higher correlation to the lifetime as the conventional one.

List of symbols

ESAH-F Electronic Analysis System of Crossing-Vehicle
ESAH-M Electronic Analysis System of Crossing-Portable
PCA principal components analysis
RCF rolling contact fatigue
S&C switches and crossings
DB Deutsche Bahn - German Railways
GPS Global Position System
ACC acceleration sensor
STFT short-time Fourier transform
SK spectral kurtosis

Acknowledgements

The authors greatly appreciate financial and technical support of Germany Railway Company (DB Systemtechnik GmbH) and WITT Elektronik GmbH.

References

[1] L. Fendrich, W. Fengler. *Handbuch Eisenbahninfrastruktur*. Second edition. Springer-Verlag Berlin Heidelberg, 2013. doi:10.1007/978-3-642-30021-9.

[2] A. Ekberg, B. Paulsson. *INNOTRACK : concluding technical report*. International Union of Railways, 2010.

[3] E. Bernal, M. Spiryagin, C. Cole. On-board condition monitoring sensors, systems and techniques for freight railway vehicles: a review. *IEEE Sensors Journal* **19**(1):4–24, 2019. doi:10.1109/JSEN.2018.2875160.

[4] U. Gerber, A. Zoll, W. Fengler. Vehicle-based assessment of wear on common crossings (in german). *EI Eisenbahningenieur* **5**:26–30, 2013.

[5] V. Kovalchuk, M. Sysyn, Y. Hnativ, et al. Development of a promising system for diagnosing the frogs of railroad switches using the transverse profile measurement method. *Eastern-European Journal of Enterprise Technologies* **92**(2):33–42, 2018. DOI:10.15587/1729-4061.2018.125699.

[6] V. Kovalchuk, M. Sysyn, J. Sobolevska, et al. Theoretical study into efficiency of the improved longitudinal profile of frogs at railroad switches. *Eastern-European Journal of Enterprise Technologies* **94**(4):27–36, 2018. DOI:10.15587/1729-4061.2018.139502.

[7] L. Xin. *Long-Term Behaviour of Railway Crossings: Wheel-Rail Interaction and Rail Fatigue Life Prediction.* PhD Thesis:. TU Delft, 2017. DOI:10.4233/uuid:7ee5405a-85f1-4bd2-b776-2013715c8783.

[8] A. Chudzikiewicz, R. Bogacz, M. Kostrzewski, R. Konowrocki. Condition monitoring of railway track systems by using acceleration signals on wheelset axle-boxes. *Transport* **33**(2):555–566, 2018. DOI:10.2478/v10174-010-0030-1.

[9] L. Brajovic, M. Malovic, Z. Popovic, L. Lazarevic. Wireless system for sleeper vibrations measurement. *Communications - Scientific Letters of the University of Zilina* **16**(4):21–26, 2014.

[10] N. O. Attoh-Okine. *Big data and differential privacy: analysis strategies for railway track engineering.* Wiley Series in Operations Research and Management Science. John Wiley & Sons, Inc., 2014.

[11] M. Sysyn, D. Gruen, U. Gerber, et al. Turnout monitoring with vehicle based inertial measurements of operational trains: a machine learning approach. *Communications - Scientific letters of the University of Zilina* **21**(2):42–48, 2019.

[12] X. Liu, V. Markiene, I. Shevtsov, R. Dollevoet. Experiment study of key parameters in turnout crossing degradation process. *Proceedings of the 10th International Conference on Contact MechanicsColorado, USA 1-3 September* pp. 122–127, 2015.

[13] L. Izvolt, J. Sestakova, M. Smalo. Analysis of results of monitoring and prediction of quality development of ballasted and ballastless track superstructure and its transition areas. *Communications - Scientific Letters of the University of Zilina* **18**(4):9–29, 2016.

[14] L. Izvolt, J. Sestakova, M. Smalo. The railway superstructure monitoring in bratislava tunnel no. 1 - section of ballastless track and its transition areas. *MATEC Web of Conferences* **117**:00063, 2017.

[15] M. Sysyn, U. Gerber, O. Nabochenko, V. Kovalchuk. Evaluation of railway ballast layer consolidation after maintenance works. *Acta Polytechnica* **59**(1):77–78, 2019. DOI:10.14311/AP.2019.59.0077.

[16] E. Martey, L. Ahmed, N. Attoh-Okine. Track geometry big data analysis: a machine learning approach. *Proceedings - 2017 IEEE International Conference on Big Data* pp. 3800–3809, 2017. DOI:10.1109/BigData.2017.8258381.

[17] M. Sysyn, U. Gerber, O. Nabochenko, V. Kovalchuk. Common crossing fault prediction with track based inertial measurements: statistical vs mechanical approach. *Pollack Periodica* **14**(1):22–36, 2019. DOI:10.1556/606.2019.14.

[18] Y. Cui, U. Martin, W. Zhao. Calibration of disturbance parameters in railway operational simulation based on reinforcement learning. *Journal of Rail Transport Planning and Management* **6**(1):1–12, 2016. DOI:10.1016/j.jrtpm.2016.03.001.

[19] S. Rapp, U. Martin, M. Strähle, M. Scheffbuch. Track-vehicle scale model for evaluating local track defects detection methods. *Transportation Geotechnics* **19**:9–18, 2019. DOI:10.1016/j.jrtpm.2016.03.001.

[20] M. Sysyn, U. Gerber, O. Nabochenko, et al. Prediction of rail contact fatigue on crossings using image processing and machine learning methods. *Urban Rail Transit* **5**(2):123–132, 2019. DOI:10.1007/s40864-019-0105-0.

[21] B. Glusberg, A. Savin, A. Loktev, et al. Counter-rail special profile for new generation railroad switch. *Advances in Intelligent Systems and Computing* **982**:571–587, 2020. DOI:10.1007/978-3-030-19756-8_54.

[22] B. Glusberg, V. Korolev, I. Shishkina, et al. Calculation of track component failure caused by the most dangerous defects on change of their design and operational conditions. *MATEC Web of Conferences* **239**:01054, 2018. DOI:10.1051/matecconf/201823901054.

[23] M. Sysyn, F. Kluge, D. Gruen, et al. Experimental analysis of rail contact fatigue damage on frog rail of fixed common crossing 1:12. *Journal of Failure Analysis and Prevention* **19**(4):in Print, 2019. DOI:10.1007/s11668-019-00696-w.

[24] M. Sysyn, O. Nabochenko, F. Kluge, et al. Common crossing structural health analysis with track-side monitoring. *Communications - Scientific Letters of the University of Zilina* **21**(3):77–84, 2019.

[25] A. Zoll, U. Gerber, W. Fengler. The measuring system esah-m (in german). *Eisenbahningenieur Kalender 2016* pp. 49–62, 2016.

[26] A. Ben, L. Saidi, S. Harrath, et al. Online automatic diagnosis of wind turbine bearings progressive degradations under real experimental conditions based on unsupervised machine learning. *Applied Acoustics* **132**:167–181, 2018. DOI:10.1016/j.apacoust.2017.11.021.

[27] A. Ben, L. Saidi, E. Bechhoefer, M. Benbouzid. Wind turbine high-speed shaft bearings health prognosis through a spectral kurtosis-derived indices and svr. *Applied Acoustics* **120**:1–8, 2017. DOI:10.1016/j.apacoust.2017.01.005.

[28] J. Antoni. Fast computation of the kurtogram for the detection of transient faults. *Mechanical Systems and Signal Processing* **21**(1):108–124, 2007. DOI:10.1016/j.ymssp.2005.12.002.

[29] MathWorks Deutschland. Matlab documentation. `https://de.mathworks.com/help/signal/ref/pkurtosis.html`.

[30] J. Coble. *Merging data sources to predict remaining useful life - an automated method to identify prognostics parameters.* PhD Thesis:. University of Tennessee, 2010.

[31] I. Jolliffe. *Principal component znalysis*. Springer series in statistics. Springer-Verlag New York, 2002. doi:10.1007/b98835.

[32] N. Attoh-Okine, A. Lasisi. Principal components analysis and track quality index: a machine learning approach. *Transportation Research Part C: Emerging Technologies* **91**:230–248, 2018. doi:10.1016/j.trc.2018.04.001.

[33] T. Hastie, R. Tibshirani, J. Freidman. *The elements of statistical learning: data mining, inference, and prediction*. Second edition. Springer-Verlag New York, 2009. doi:10.1007/978-0-387-84858-7.

[34] M. Trauth. *MATLAB recipes for earth sciences*. fourth edition. Springer-Verlag Berlin Heidelberg, 2015. doi:10.1007/978-3-662-46244-7.